Central Power Research Institute

Vol. 20(2)/235-242, December 2024
ISSN (Print) : 0973-0338
DOI : 10.33686/pwj.v20i2.1181

Power Research

Development and Testing of HTS Double Pancake Coil for SMES Application

A. Anand[1*], A. S. Gour[1], T. S. Datta[1], U. Bhunia[2] and V. V. Rao[1]

[1]Cryogenic Engineering Center, IIT Kharagpur, Kharagpur – 721302, West Bengal, India

[2]VECC Kolkata, Department of Atomic Energy, Kolkata – 700064, West Bengal, India; ankit5088@gmail.com

Abstract

Superconducting Magnet Energy Storage (SMES) stores energy in the form of magnetic energy and has very high cycle efficiency compared with other Energy Storage Systems (ESS). It is being used in many power applications, such as instantaneous voltage drop compensation, dampening low frequency, load fluctuation compensation, and pulsed power sources. Recently 2G High-Temperature Superconductors (HTS) have been used for making modular SMES coils in the form of double pancakes, which can be easily assembled as solenoid and toroid. A single double pancake coil is wound using SuNAM make SCNk04200. Fabrication details of each component of the HTS DP coil are presented. The design of the in-house HTS tape insulation using Kapton, DP winding mechanism, which can provide the pretension during winding, and vacuum impregnation are presented. The test setup of testing the DP coil is also provided. The DP coil is tested for I-V characterization and central magnetic field. A Numerical model is also validated using the experiment for future design of large-scale SMES. The comparison is done for the central magnetic field and maximum operating current.

Keywords: Double Pancake, Energy Storage, HTS, Superconducting Magnet, Winding

1. Introduction

Superconducting Magnet Energy Storage (SMES) applications can be used in power grids[1-3] for voltage levelling, dampening low frequency, load fluctuation compensation, Uninterrupted Power Supply (UPS)[4], and pulsed power sources. SMES stores energy in the form of a magnetic field and can release the energy in a fraction of a second with very high cyclic efficiency[5]. Figure 1 shows a typical SMES connected to the grid via 3 phase line. The superconducting coil is inside the cryostat. Due to the superconducting nature of the coil, there is no joule heating during energy storage. Many projects have been undertaken around the world for both Low-Temperature Superconductor (LTS) SMES as well as High-Temperature Superconductor (HTS) SMES[6,7]. The 2nd Generation (2G) HTS tape has thin tape-like structures and is superior to LTS wires due to high current carrying capacity in the presence of a high magnetic field[8,9]. These thin tape-like composite structures can be wound in the form of a Double Pancake (DP) coil, which can be assembled in the form of a solenoid or toroid[10,11]. Both types of SMES are already built and tested for storage capacity ranging from 4 kJ to 100 MJ[12,13]. The operating temperature for various worldwide projects varied from 4.2 K to 30 K[14,15].

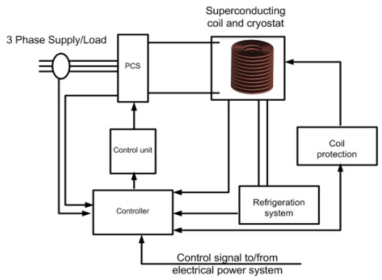


Figure 1. Schematic of SMES system.

This paper describes the complete construction of a single DP module of magnet coil along with the testing result. Section 2 gives the component details of the DP coil. HTS tape insulation wrap using Kapton is given in Section 3. The In-house DP winding machine is described in Section 4. It also includes the tightening mechanism details, which were used to provide pretension in the DP coil during winding. Section 5 gives the

*Author for correspondence

© Power Research

details about the vacuum impregnation setup. The DP winding steps and final DP coil are given in Section 6. Section 7 presents the test setup used for testing along with the result. Validation of the numerical model based on the same geometry is given in Section 8. Comparisons between experiments and simulation are given in Section 9. Section 10 concludes the paper.

2. Coil Design

The DP coil configuration was chosen as it has both terminals outside, thus making it easier to connect with neighbouring coils. Moreover, the joining of two DP coils will take place in the lower magnetic field, which is outside the coil, rather than inside, where a high magnetic field is present. Figure 2 shows the general exploded view of DP coil components, excluding lead connections.

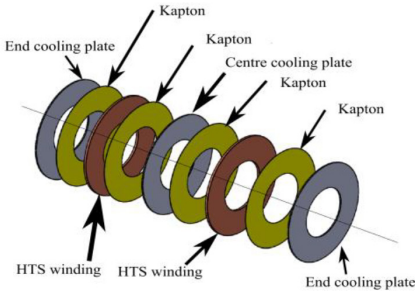


Figure 2. Stacking details of DP coil.

Copper is selected to make the bobbin and cooling plate due to high thermal conductivity. Figure 3(a) shows the copper bobbin of the DP coil. A central groove accommodates the centre plate, which can be fixed using bolts. Figure 3(b) shows that the centre plate has two parts. One part has a slot to allow for the crossover of HTS tape from one side to the other. Figure 3(c) shows the assembly of the centre plate and copper bobbin. The top and bottom cooling plates are shown in Figure 3(d). These cooling plates are assembled into a bobbin after the winding is completed. The SuNAM SCNk04200 2G HTS tape specification and dimensions are given in Table 1. The total thickness of HTS tape, including Kapton thickness, was 0.17 mm.

Table 1. Specification of HTS tape and fabricated coil major dimensions

Parameters	Value
HTS tape width	4[mm]
HTS tape thickness including insulation	0.17[mm]
Outer dia of former	80[mm]
Number of turns	84
Copper plate thickness	2[mm]
Outer dia of coil winding	108[mm]

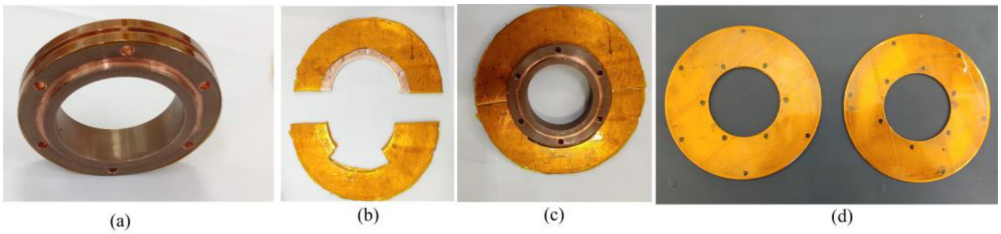


Figure 3. Photograph of **(a)** copper former **(b)** Center plate **(c)** assembled view of the centre plate and former **(d)** Top and bottom plate.

3. HTS Tape Kapton Wrap Mechanism

HTS tape needs to be wrapped with suitable material to provide layer-wise insulation. Kapton tape is the favoured material for insulation HTS tape due to its lower thickness and high dielectric constant. The Kapton is wrapped in the HTS tape in a helical fashion, having overlap in the Kapton tape.

An in-house HTS tape wrapping machine using Kapton tape was fabricated. Figure 4 shows the photograph of the Kapton tape wrap machine. The manufactured spool can be mounted directly in the fixture. This spool can rotate freely along its axis. The tape is passed through a guide and a tensioner before wrapping. The tensioner provides tension to tape to avoid slacking during the wrap operation. The linear motion of tape and circular motion of Kapton tape is performed with the help of two independent DC motors: Arduino MEGA 2560 controls both the DC motors via a separate motor controlled based on PWM. During the wrapping, the linear speed of HTS tape increases for the fixed rotation speed of the motor due to the increase in

winding radius; hence, the circular motion of Kapton needs to be varied accordingly. The program written in Arduino takes care of this issue by automatically adjusting the speed of the motors. The speed of both motors was measured in real-time by using the hall sensors encoder housed in both DC motors. This helps in monitoring the winding process. The spool, which will have the Kapton insulated HTS tape, has the capacity of a minimum of 100 m. The Kapton tape is mounted on a rotating arm, free to rotate about its axis. The angle of the Kapton tape can be adjusted according to the overlap required.

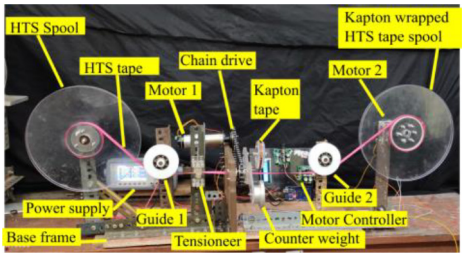


Figure 4. HTS tape insulation by wrapping the Kapton tape helical mechanism.

4. DP Winding Machine Sections

DP winding machine is required to wind a DP magnet coil. The design of a winding machine is made by considering the following factors:

1. Provision to mount the spool from the manufacturer and transfer it to a custom-made spool.
2. Divide the total length of tape into two spools equally.
3. Winding can be performed easily with the number of turns counting.
4. Provision for pretension on HTS tape during winding.
5. If required, it can co-wind turn-by-turn insulation and supporting layers (stainless steel or brass tape).

Based on these factors, a DP winding machine was designed. A detailed 3D drawing of this winding machine is shown in Figure 5. A photograph of developed in-house DP winding is shown in Figure 6.

The removal support stand in Figure 5(a) will hold the manufacture spool to transfer the HTS tape to the custom spool. The counter is used to calculate the length transferred. The number of turns required for transferring L length can be calculated by solving the quadratic equation given by Equation (1). The one positive solution of a quadratic equation can be calculated by the simple expression given by Equation (2).

$$n_r^2 * t + n_r * ID - \frac{L}{\pi} = 0 \tag{1}$$

$$n_r = \frac{-ID + \sqrt{ID^2 + 4 * t * \frac{L}{\pi}}}{2 * t} \tag{2}$$

In case (2) gives a fractional solution, n_r can be rounded to the nearest integer.

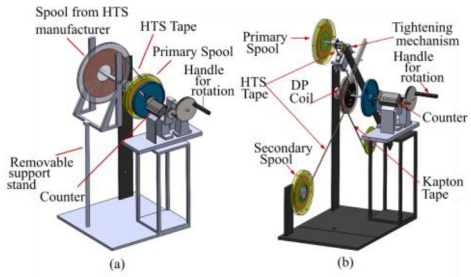


Figure 5. **(a)** 3D CAD drawing for transferring tape from manufacturer spool to primary spool and primary spool to secondary spool, **(b)** 3D CAD drawing for DP winding machine.

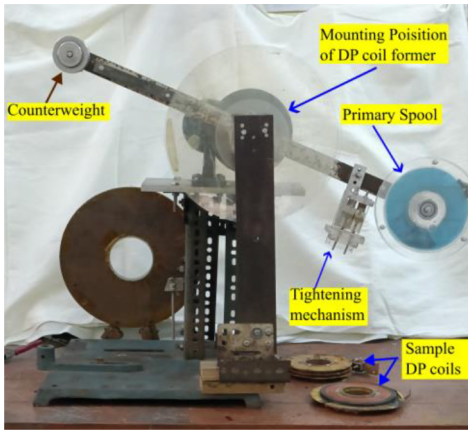


Figure 6. Photograph of DP winding machine.

The custom spool can be again mounted on a removable stand to divide the required length equally into two halves. Once the HTS tape is divided into two spools equally, the removable stand needs to be removed from the winding machine. Figure 5(b) will be used to wind the DP coil. The tightening mechanism is responsible for providing pretension during winding. This prevents the sagging of HTS tape during winding. Soft felt material does not damage the HTS tape while providing ample tension by pressing it. Figure 7 shows the 3D CAD of the tightening mechanism. The pretension applied by this

was 2N. The value is calculated by simple kinetic friction measurement of sliding HTS tape, *i.e.*, the force measured during the sliding of HTS tape through the winding machine.

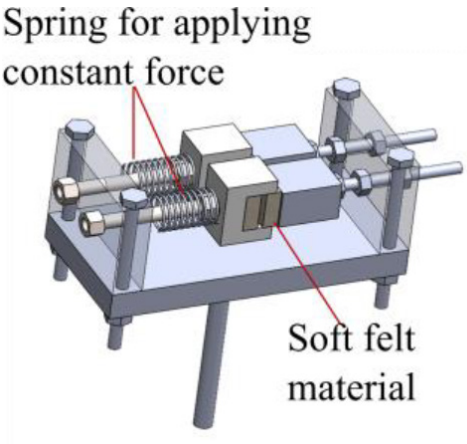


Figure 7. Tightening mechanism to provide pretension in DP coil during winding.

5. Vacuum Impregnation Unit

During the operation of SMES, a high operating current will produce a large Lorentz force. In the absence of any bonding between layers, it can release strain energy due to the movement of layers, leading to an induced high voltage between layers, which will result in a sudden release of energy in the form of a spark, thus causing the quench of the magnet[16]. Vacuum impregnation is one method that is used in electrical machines like motors and transformers to stop individual strands of wire from moving. It was decided to use vacuum impregnation to bond all the turns together.

A vacuum desiccator that stores materials under a vacuum is modified to work as a vacuum impregnation vessel. A schematic of vacuum impregnation is shown in Figure 8(a). A butterfly valve is present to cut off the vacuum pump from the chamber whenever required. The ball valve can be operated manually to allow the varnish to enter the chamber when required. An electric bulb was also attached to the chamber to heat the DP coil after vacuum impregnation. The power of the bulb can be controlled using a variac. With a variac and a temperature sensor, the coil's temperature can be kept constant during drying. Figure 8(b) shows the photograph of the vacuum impregnation unit.

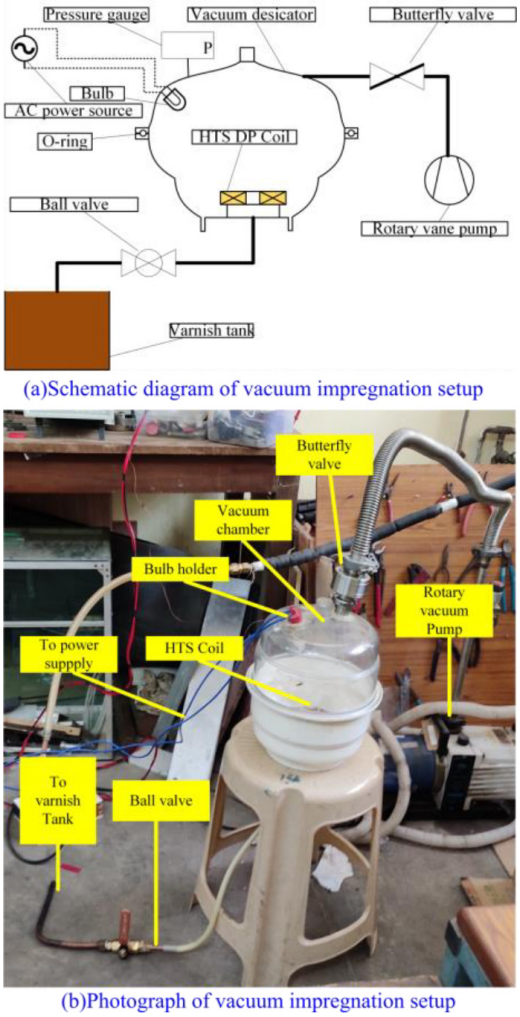


Figure 8. Schematic and photograph of vacuum impregnation setup.

6. DP Coil

The DP coil was used using the winding machine. Figure 9(a) shows the primary spool having a total length of 50 m HTS tape. This total length was divided equally into two spools. Figure 9(b) shows the equally distributed HTS tape in the primary and secondary spool. Figure 9(c) shows the crossover of HTS tape into either side of the DP coil. Since the middle plate consists of two parts, HTS tape was first crossed through the slot through one of the parts, and after both the parts were assembled. Figure 9(d) shows the final wound DP coil using the winding machine. The top and bottom acrylic sheets were used, which were later replaced by copper plates.

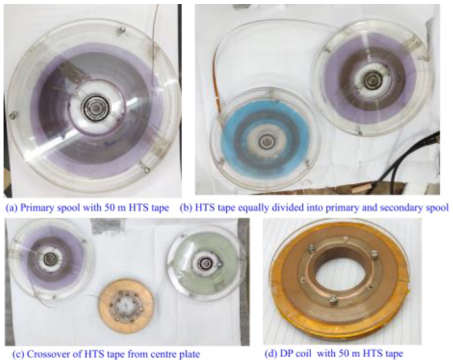


Figure 9. DP coil fabrication process.

7. Testing for IV Characterization and Central Magnetic Field of COI

After the winding of the DP coil, the top and bottom acrylic plates were replaced with the copper cooling plate. For the coil to be tested for the I-V and central magnetic field, a suitable current lead was connected to HTS tape. Due to the difference between the dimension of the HTS tape and the current lead from the power supply, the coil was fixed on a platform, having a fixed current lead structure. The end terminal of the DP coil was soldered to these leads; thereby, the weight and orientation of current leads from the power supply do affect the terminals of the DP coil. Figure 10 shows the DP coil with electrical connections. It also shows the voltage leads directly soldered to HTS tape terminals.

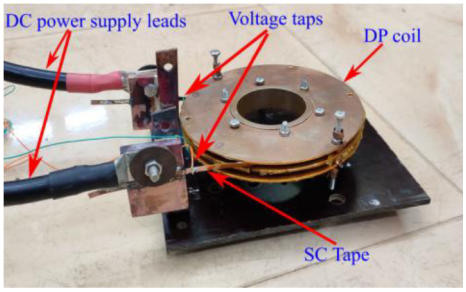


Figure 10. DP coil with electrical connection before testing.

Figure 11 shows the schematic of testing I-V characterization and central magnetic field. The I-V characterization and measurement of the central magnetic field at the rated current was performed at 77 K using liquid nitrogen. The coil was fully submerged in liquid nitrogen during testing. A Keithley multimeter (Model No 2450), which can measure the voltage in micro-volts, was used to measure the voltage across the DP coil. A Lake Shore Teslameter (Model No: F41) with a cryogenic probe was used to measure the central magnetic field. Figure 12 shows the I-V characterization plot for the DP coil with a DC power supply. 1 μV/cm criteria were used to determine the maximum allowable current, and for 50 m total HTS tape, it comes out to be 5 mV. The maximum allowable operating current obtained was 70 A. The central magnetic field corresponding to 70 A was 0.158 T.

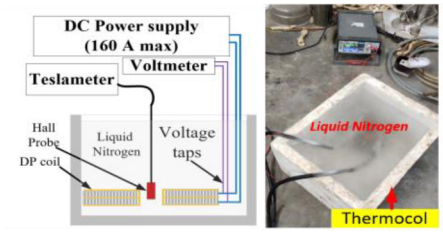


Figure 11. Schematic of I-V characteristic and central magnetic field test.

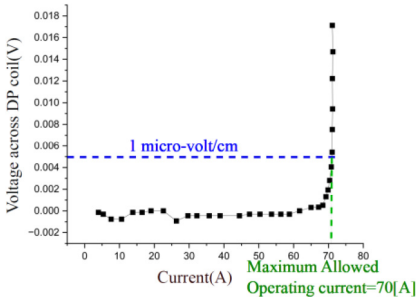


Figure 12. I-V characteristic of DP coil with DC supply.

8. Validation of the Numerical Model

Fabrication of SMES coil is a costly process, and once fabricated, it is not possible to change the dimension of the coil. The coil is designed based on many parameters, such as stored energy, cryostat dimension, cooling methods, *etc*. It is important to have the numerical simulation of magnetic fields and optimized coil dimensions concerning minimum cost before fabrication. However, the accuracy of the optimized model depends upon the accuracy of the numerical model. A numerical model based on the fabricated geometry allows us to design a big SMES coil. For this reason, a numerical model is simulated for the same coil on which experiment results have been presented. For numerical simulation, COMSOL Multiphysics was used.

An axis-symmetric geometry was created with the exact dimensions of the coil, as given in Table 1. The coil was bound by air as the magnetic field extended far beyond the coil dimension. The air has the same relative permeability as liquid nitrogen; hence, it will not affect the magnetic field calculation. Figure 13 shows the layer-wise geometry made in COMSOL. Total HTS tape thickness, including Kapton, was 0.17 mm. Kapton insulation was not modelled and was replaced by an air gap in geometry, which can be seen as a gap between turns. The model is solved two times, first for the determination of operating current and 2nd for the determination of magnetic flux density, inductance, and stored energy. Figure 14 shows the complete flow chart for numerical simulation.

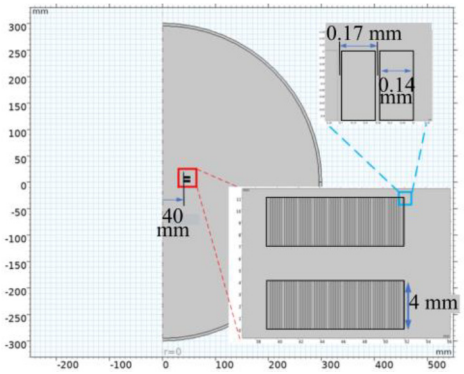


Figure 13. Axis-symmetric geometry in comsol for verification.

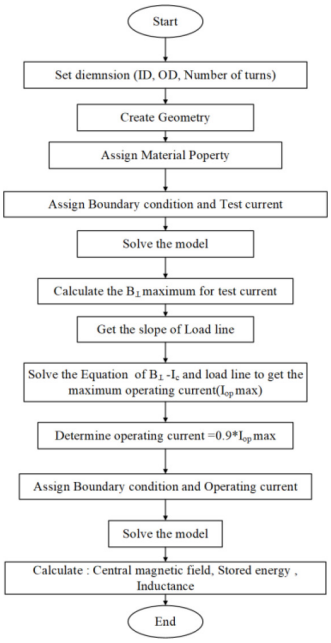


Figure 14. Flowchart for numerical simulation of magnet coil.

8.1 Calculation of Operating Current

The operating current depends upon the coil geometry and B-I character of the selected HTS tape[17,18]. B-I characteristic of SuNAM SCNk0400 is shown in Figure 15 and was taken from[19]. The curve-fitted exponential coefficient is also given in this figure. A test current was used to calculate the maximum B_r values in whole coils[20,21]. After the creation of geometry, superconductor and surrounding region material property was provided. The excitation current was set as the test current. Engineering current density was provided to HTS tape, *i.e.*, even though the superconducting layer was only 1 micrometre thick and responsible for current-carrying, the current was assumed to be flowing through all the layers uniformly. The mesh operation was performed within COMSOL. An extremely fine element was chosen for this operation. The model was solved for magnetic vector potential given by Equation (3). Magnetic flux density was calculated using Equation (4).

$$\nabla \times \left(\frac{1}{\mu} \nabla \times \mathbf{A} \right) = \mathbf{J} \tag{3}$$

$$B = \nabla \times \mathbf{A} \tag{4}$$

B_r maximum was calculated for the whole geometry of the coil which interestingly comes out to be the top surface of the coil. Test current divided by B_r max provides load line slope given by Equation (5). With this load line slope, an equation of the line was derived by passing through the origin. The load line equation and curve fitted B⊥ – I curve were solved simultaneously as given by Equation (6). Here, a(T), b(T), c(T), and d(T) are the curve fit coefficients depending upon the temperature. Equation (6) was solved using the Newton-Rapson method within the COMSOL to determine the point of intersection. COMSOL allows to have this program in JAVA. Using Equation (7), the maximum operating current can be calculated by B⊥ at the point of intersection. The operating current Equation (8) was taken as 90 per cent of the maximum possible value for safety reasons.

$$m = \frac{I_{\text{test}}}{B_r max} \tag{5}$$

$$a(T)e^{b(T)B_\perp} + c(T)e^{d(T)B_\perp} - m * B_\perp = 0 \tag{6}$$

$$I_{opmax} = a(T)e^{b(T)B_\perp max} + c(T)e^{d(T)B_\perp max} \tag{7}$$

$$I_{op} = 0.9 * I_{opmax} \quad (8)$$

The maximum operating current (I_{opmax}) obtained was 69.7 A.

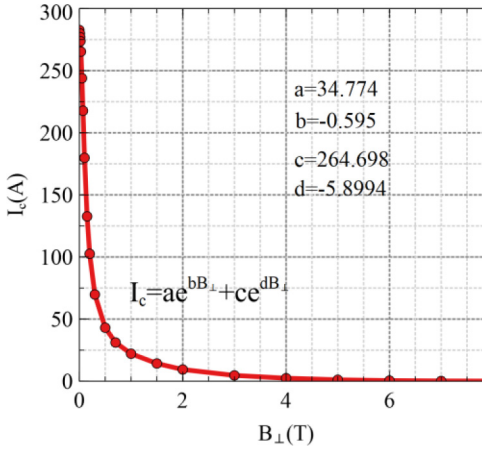


Figure 15. B⊥ – Ic characteristic of HTS tape at 77 K.

8.2 Calculation of Magnetic Flux Density Distribution

After getting the operating current, this current was set as a parameter in COMSOL. The simulation was performed for a known operating current. Magnetic field distribution, inductance, and stored energy were calculated after solving the model. Figure 16 shows the magnetic flux density plot of the magnet coil. The magnetic density at the centre of the coil was lower than the magnetic flux density at the inner wall.

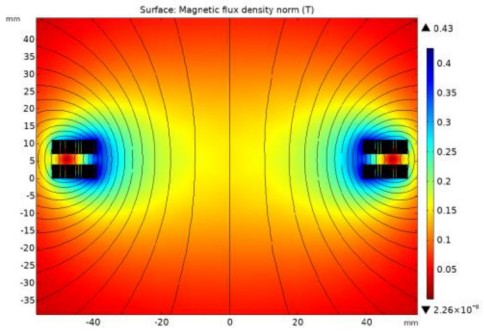


Figure 16. Magnetic flux density surface plot at 69.7 A.

9. Comparison between Experiment and Simulation

The experimental results of magnet coil testing in liquid nitrogen at 77 K using a DC power supply were compared with the numerical simulation for the maximum operating current and central magnetic field. The maximum operating current was determined based on the voltage difference across the coil terminal. For the length of 50 m HTS tape, it was 5 mV using 1 μV/cm criteria. During the testing, the DC was increased slowly, and the moment voltage across the terminal reached 5 mV; this current maximum operating current. At this instant, the central magnetic field was measured. In simulation, the operating current procedure was discussed in Section 7.1. Table 2 shows the comparison of both values. The simulation results are very near to the experimental result, having an error percentage of 1 %.

Table 2. Comparison between experiment and numerical evaluation

	Experiment	Simulation	% error
$I_{op\ max}$(A)	70	69.7	0.4
B0 [T]	0.158	0.159	0.6

The comparison shows that the method used to simulate one single coil can be extended to the design of large-scale magnet coil not only limited to SMES but for other solenoid coils used in applications such as MRI and high field NMR, which utilized DP solenoid coil. Although the comparison is performed for 77 K, the numerical technique is easily extended to other operating temperatures by selecting the curve fit coefficient of the B-I characteristic at that temperature to determine the operating current. For large magnet coils, further simplification in simulation can be done using quarter-axis symmetric geometry.

10. Conclusions

A 2G HTS superconducting magnet coil prototype was fabricated using an in-house DP winding machine and tested for I-V characterization and central magnetic field at 77 K using liquid nitrogen. The DP coil was wound using 50 m of HTS. The maximum operating current obtained was 70 A with a voltage difference of 5 mV. The measured central field at 70 A operating current was 0.158 T. A numerical model of the fabricated coil is also validated in terms of operating current and central magnetic field. There was a 0.6 % error between the experiment and the simulation. This validation will help in designing a large-scale superconducting magnet coil with accuracy.

11. References

1. Sharma R. Other applications of superconducting magnets. Superconductivity; 2021. p. 549-620.https://doi.org/10.1007/978-3-030-75672-7_12
2. Iwasa Y. Superconducting magnet technology. Case Studies in Superconducting Magnets; 2009. p. 1-24. https://doi.org/10.1007/b112047_1
3. Maeda H, Yanagisawa Y. Recent developments in high-temperature superconducting magnet technology (Review). IEEE Trans Appl Supercond. 2014; 24(3):1-12. https://doi.org/10.1109/TASC.2013.2287707
4. Kreutz R, Salbert H, Krischel D, Hobl A, Radermacher C, Blacha N, *et al*. Design of a 150 kJ high-Tc SMES (HSMES) for a 20 kVa uninterruptible power supply system. IEEE Trans Appl Supercond. 2003; 13(2):1860-2. https://doi.org/10.1109/TASC.2003.812929
5. Hawley CJ, Gower SA. Design and preliminary results of a prototype HTS SMES Device. IEEE Trans Appl Supercond. 2005; 15(2):1899-902. https://doi.org/10.1109/TASC.2005.849328
6. Dai S, Xiao L, Wang Z, Zhang J, Zhang D, Hui D, *et al*. Design of a 1 MJ/0.5 MVA HTS Magnet for SMES. IEEE Trans Appl Supercond. 2007; 17(2):1977–80. https://doi.org/10.1109/TASC.2007.899194
7. Xiao NL, Wang NZ, Dai NS, Zhang NJ, Zhang ND, Gao NZ, et al. Fabrication and Tests of a 1 MJ HTS Magnet for SMEs. IEEE Trans Appl Supercond. 2008; 18(2):770-3. https://doi.org/10.1109/TASC.2008.922234
8. Tixador P, Bellin B, Deleglise M, Vallier JC, Bruzek CE, Allais A, Saugrain JM. Design and first tests of a 800 kJ HTS SMES. IEEE Trans Appl Supercond. 2007; 17(2):1967-72. https://doi.org/10.1109/TASC.2007.898520
9. Bellin B, Tixador P, Deleglise M, Vallier JC, Pavard S, Bruzek CE. Cryogenic design of a 800 kJ HTS SMES. J Phys Conf Ser. 2006; 43:817-2. https://doi.org/10.1088/1742-6596/43/1/199
10. Wojtasiewicz G, Janowski T, Kozak S, Kondratowicz-Kucewicz B, Kozak J, Surdacki P, *et al*. HTS magnet for 7.3 kJ SMES system. J Phys Conf Ser. 2006; 43:821-4. https://doi.org/10.1088/1742-6596/43/1/200
11. Kim WS, Kwak SY, Lee JK, Choi KD, Jung HK, Seong KC, *et al*. Design of HTS magnets for a 600 kJ SMES. IEEE Trans Appl Supercond. 2006; 16(2):620-3. https://doi.org/10.1109/TASC.2005.864244
12. Zheng J, Peng SS, Li WY, Dai YJ. Magnet design of 10MJ multiple solenoids SMES. OP Conf Ser: Earth Environ Scz. 2019; 233:032026-6. https://doi.org/10.1088/1755-1315/233/3/032026
13. Ciceron J, Badel A, Tixador P, Forest F. Design considerations for high-energy density SMES. IEEE Trans Appl Supercond. 2017; 27(4):1-5. https://doi.org/10.1109/TASC.2017.2655627
14. Vialle J, Badel A, Tixador P, Ciceron J, Forest F, Pasquet R. Preliminary tests of pancakes from a 12 T REBCO insulated solenoid magnet. IEEE Trans Appl Supercond. 2021;31(5):1-5. https://doi.org/10.1109/TASC.2021.3057837
15. Vialle J, Badel A, Tixador P. 12 T insulated REBCO magnet used as 1 MJ SMES: Protection strategies and preliminary assembly tests. IEEE Trans Appl Supercond. 2022; 32(6):1-7. https://doi.org/10.1109/TASC.2022.3180979
16. Morandi A, Gholizad B, Fabbri M. Design and performance of a 1 MW-5 s high temperature superconductor magnetic energy storage system. Supercond Sci Technol. 2015; 29(1):015014. https://doi.org/10.1088/0953-2048/29/1/015014
17. Li Y, Song P, Kang Y, Feng F, Qu T. Design of a 30-K/4-kJ HTS magnet cryocooled with solid nitrogen. IEEE Trans Appl Supercond. 2018; 28(4):1-6. https://doi.org/10.1109/TASC.2018.2814960
18. Anand A, Gour AS, Datta TS, Rao VV. 50 kJ SMES magnet design optimization using real coded genetic algorithm. IOP Conf Ser Mater Sci Eng. 2022; 1240(1):012137-7. https://doi.org/10.1088/1757-899X/1240/1/012137
19. Wimbush SC, Strickland NM. A public database of high-temperature superconductor critical current data. IEEE Trans Appl Supercond. 2017; 27(4):1-5. https://doi.org/10.1109/TASC.2016.2628700
20. Anand A, Gour AS, Datta TS, Rao VV. Study on HTS SMES coil for optimized dimensions. IEEE Trans Appl Supercond. 2023; 33(7):1-11. https://doi.org/10.1109/TASC.2023.3289092
21. Anand A, Gour AS, Datta TS, Rao VV. Novel-shape-based HTS magnet coil for SMES application. J Supercond Nov Magn. 2023; 36(4):1121-31. https://doi.org/10.1007/s10948-023-06547-y